Nanoscale

Prediction of water transport properties on the anisotropic wetting surface via deep learning

Journal:	*Nanoscale*
Manuscript ID	NR-ART-06-2023-002709
Article Type:	Paper
Date Submitted by the Author:	08-Jun-2023
Complete List of Authors:	Guo, Yuting; Tohoku University Institute of Fluid Science, ; Sun, Haiyi; Tohoku University, Institute of Fluid Science An, Meng; The University of Tokyo, Department of Mechanical Engineering Mabuchi, Takuya; Tohoku University, Zhao, Yinbo; Tongji University, School of Aerospace Engineering and Applied Mechanics Li, Gaoyang; Tohoku University,

Prediction of water transport properties on the anisotropic wetting surface via deep learning

Yuting Guo[a#], Haiyi Sun[a#], Meng An[b], Takuya Mabuchi[a,c], Yinbo Zhao[a], Gaoyang Li[a*]

[a] Institute of Fluid Science, Tohoku University, 2-1-1 Katahira, Aoba-ku, Sendai 980-8577, Japan

[b] Department of Mechanical Engineering, Graduate School of Engineering, The University of Tokyo, 7-3-1, Bunkyo-ku, Tokyo113-8656, Japan

[c] Frontier Research Institute for Interdisciplinary Sciences, Tohoku University, 2-1-1 Katahira Aoba-ku, Sendai, Miyagi 980-8577, Japan

* Corresponding author: Gaoyang Li

# These authors contributed equally to this work.

E-mail: li.gaoyang.e4@tohoku.ac.jp

Abstract

Understanding the water flow behavior on an anisotropic wetting surface is of practical significance in nanofluidic devices for their performance improvement. However, current methods of experiments and simulations face challenges to measure in real time and visually display the water transportation. Here, molecular dynamics simulation was integrated with our developed multi-attribute point cloud dataset and customized network of deep learning to achieve the mapping from the anisotropic wetting surface to static and dynamic behaviors of water molecules and realize the high-performance prediction of water transport behavior. More importantly, for the chaotic phenomenon of water molecule flow caused by thermal fluctuation and limited sampling, we proposed a nanoparticle tracking optimization strategy to improve the prediction performance of velocity field. The prediction results proved the deep learning framework proposed in this work owned superior performance in accuracy, computational cost and visualization, and had the potential of generality to model transport behavior of different molecules. Our framework can be expected to motivate the development of real-time water flow prediction at interface and contribute to the optimization and design of surface structures in nanofluidic devices.

Keywords

Nanofluidic; Wettability; Deep learning; Nanoparticle tracking strategy; Real-time visualization

1. Introduction

With the advance of nanotechnologies, nanofluidic as a new frontier of fluid science and engineering has received increased attention in fields ranging from the bioengineering, drug discovery, energy and environmental engineering to the optical property tuning [1]. When the fluid flow approaches the nanoscale ranging from 1 to 100 nm, the properties of flow become unique. Different from fluid flow at the macroscale, effects of gravity and inertia on fluid flow at the nanoscale can be ignored and the molecular behavior at the solid-liquid interface becomes dominant on controlling the transportation [2]. Understanding the fluid flow at the nanoscale is increasingly crucial for the design and fabrication of various nanofluidic devices.

Transport phenomena of fluids on carbon nanostructures, such as the velocity slip and the flow rate of water, have been widely studied using experimental and simulation methods in the past [3–6]. Simultaneously, molecular dynamics (MD) method has provided the useful platform and knowledge for elucidating the nanoscale phenomena [7,8]. A lot of MD studies focused on the investigation into profiles of liquid flow at carbon surface [9–12]. In real applications, graphene is usually coated by a variety of metals, ceramics, and polymers [13]. At such case, the physical discontinuity or chemical heterogeneity on such solid surface can consequently lead to the anisotropic wettability. If different parts of a surface own different physical and chemical properties, the distribution of liquid on the surface can be heterogeneous, which consequently has effects on the fluid flow properties at the interface. Although the study of water transport and diameter-dependent slippage has moved forward significantly, high economic cost of experiments like the generation of various striped

patterned surfaces, and high computational cost of MD simulations significantly hinder the further investigation on the interfacial flow properties at the anisotropic wetting substrate.

Recently, data-driven deep learning algorithms show great advantages over traditional methods in several fields due to their low computational cost and high accuracy [14–24]. Although a large amount of researches have explored the application of deep learning to the nanoscale, these deep learning frameworks usually focused on the solid by extracting low-dimensional feature vectors to characterize the microscopic structure of ordered crystal [25], but the effective extraction of microscopic features of liquids faced challenges. In our previous work, point features of liquids were extracted in large quantities to succeed in predicting the two-dimensional (2D) distribution of density and temperature for liquids using our developed deep learning frameworks [26,27]. Due to irregular surface geometry in flow channel, we proposed a three-dimensional (3D) deep learning network to accurately characterize the fluid flow properties in three dimensions, which sampled with dual channels and input multiple attributes of 3D data to extract structural characteristics of the anisotropic wetting substrate and the fluid dynamic properties.

In this study, datasets were built using molecular dynamics (MD) simulation, and deep learning approach was applied primarily to reveal both static (adsorption density distribution) and dynamic properties (fluid flow behaviors) of water molecules on the anisotropic wetting surface. Different distributions of hydrophilic platinum (Pt) on hydrophobic graphene were chosen to form an anisotropic wetting surface. The atomic/molecular input disorder issue of multibody system was solved. In addition, for the insufficient sampling of water molecular

velocity field based on MD simulated chaotic system, a customized nanoparticle tracking optimization strategy was proposed to adapt to different modeling tasks and helped to achieve more regular and stable prediction performance. Compared with the previous simulation work, the algorithm of deep learning in this work significantly reduced the computational cost. It took less than 1 second to complete the real-time mapping from the geometry structure of anisotropic wetting surface to the transport properties of water flow, as well as the visually output of the water adsorption behavior. The network structure has been used for thermodynamic prediction, while has not been applied to model fluid flow systems at solid-liquid interface, which asked for datasets produced from MD simulation, training and testing of network and the interpretation of nanoparticle tracking optimization strategy. Some sets of deep learning predictions were displayed to take an insight into the landscape with high-level anisotropic interaction (referred to adsorption and flow of water molecules) between Pt/graphene substrate and water molecules. This work significantly indicated that the emerging paradigm in the field of nanofluidic is shifting to the visualization in real time, analysis based on the big data and the related disciplines where new knowledge is being learned, which can broaden the horizon of investigation into artificial surfaces with specific wetting properties and help to design microfluidic devices.

2. Methods

2.1. Simulation models and initial configuration

We used molecular dynamics method to construct the liquid flow system, where

Pt/graphene acted as substrates and their anisotropic wetting surfaces can significantly affect interfacial transport properties of liquid [28–33]. The developed modified Martini force field [34–37] was used to construct the water and Pt/graphene surfaces, which was shown in Figure 1. We used coarse-grained model to study the molecular flow because the obtained flow patterns was smooth [38]. The velocity distribution of the water model with an explicit hydrogen atom would be subject to great measurement error due to the light mass [30]. In addition, the Martini force field tunes hydrophobicity and hydrogen bond properties by different parameterizations of the Lennard-Jones and the electrostatic interactions. Therefore, the effect of hydrogen bond that plays a key role in water flow at nanoscale has been included into the water model of Martini force field. Therefore, the Martini force field was assumed to be applicable to the present study.

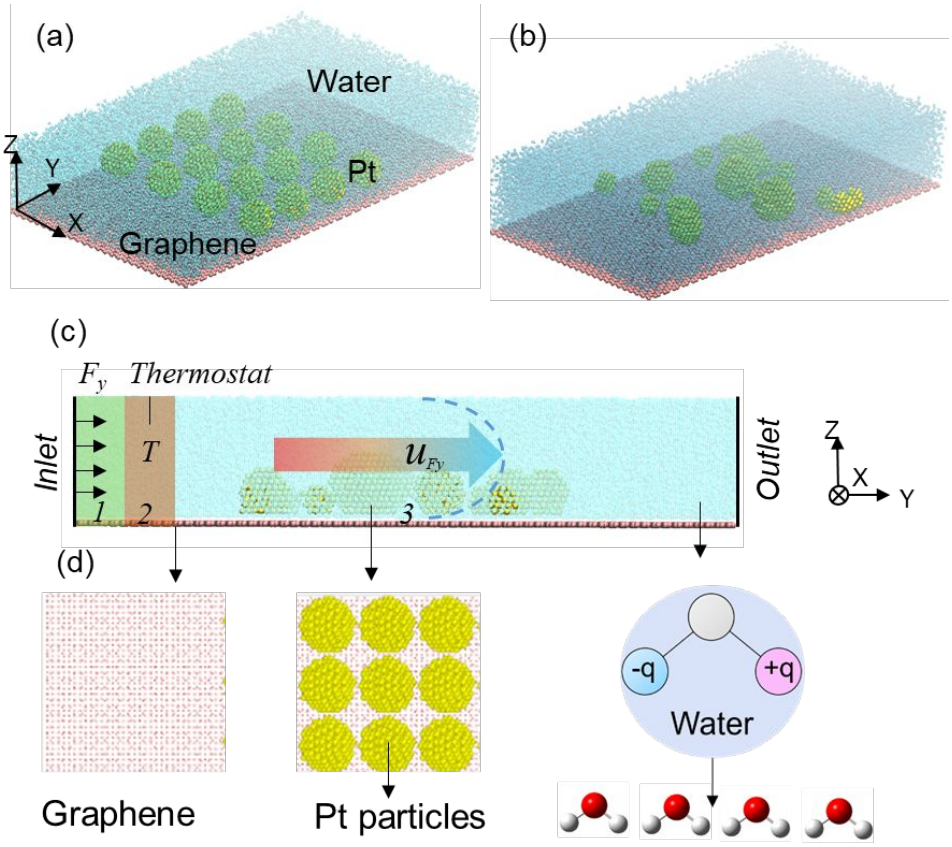

Figure 1. Water flow models where (a) Pt particles of the same size uniformly distribute on the graphene substrate. (b) Pt particles of the same size randomly distribute on the graphene substrate. (c) Domain of water flow from inlet to outlet containing three independent regions to drive flow, control inlet temperature and collect data. (d) The water, graphene, and Pt models.

In our force field, the nonbonded interactions are described as:

$$\phi(r_{ij}) = 4e_{ij}[(\frac{\sigma_{ij}}{r_{ij}})^{12} - (\frac{\sigma_{ij}}{r_{ij}})^{6}] + \frac{q_i q_j}{4\pi\varepsilon_0 r_{ij}} \quad (2)$$

The bonded interactions are expressed as:

$$\phi(r) = \frac{1}{2}k_r(r - r_0)^2 \quad (3)$$

and the bending is described as:

$$\phi(r) = \frac{1}{2}k_\theta[cos(\theta) - cos(\theta_0)]^2 \quad (4)$$

According to our previous work, refined polarizable water model [39] was selected, in which four water molecules were simplified as a coarse-grained (CG) bead. Type N_{da} bead in this work was chosen as the Pt particle and its contact angle of θ was about 23°, which was close to 25° contact angle of water-Pt at 300K in the experiment [40]. Type C_5 bead represented the graphene substrate, and its contact angle was about 119.95°. Interaction parameters of simulation setting can refer to our previous study [33,34]. The surface area of graphene was 200 × 400 Å^2 for all models.

We constructed different substrate models. Firstly, in order to accurately quantify the influence of the size of Pt particles, as well as their distribution, on water flow, we assumed that Pt particles of the same size uniformly distributed on the graphene substrate, which was shown in Figure 1(a). In addition to these setting with regular distribution, we created

systems with randomly distributed Pt particles, each with a different number of Pt particles of different size (2-4nm), as detailed in Table 1. With our setting, effects of the Pt/graphene substrate structure on the surface wettability, as well as the corresponding fluid flow behavior at interface, were investigated.

Table 1. The details of the Pt/graphene substrate for uniform and random distribution of Pt particles and the sample number for the training set and test set*.

Type	Diameter range [nm]	Pt content range [wt%]	Number range of Pt particles	Pt-Pt distance range [nm]	Sample number (training set)	Sample number(test set)
Uniform	2 - 4	30 - 90	4 - 36	2.5 - 10.0	1.215×10^6	1.35×10^5
Random	2 - 4	10 - 90	2 - 64	1 - 10.0	1.215×10^6	1.35×10^5

* The parameters for Pt/graphene substrate consist of the size and number of Pt particles, the Pt content, and the distance between neighboring Pt particles (Pt-Pt distance). Pt-Pt distance in uniform distribution was assumed to be the same in the *x* and *y* directions.

2.2. MD simulation details

All MD simulations in this work were carried out by the large-scale atomic/molecular massively parallel simulator (LAMMPS) package. All three dimensions were set as periodic boundary conditions. Water molecules dispersed in the system randomly at the initial stage, and a Pt/graphene substrate located on the system bottom in the *z*-direction. The *NPT* simulations with T = 300 K and P = 1 atm spent 50 ns compressing the system in the *z*-direction and equilibrating the system, and the time step of integration was 20 fs.

Afterwards, it took 250 ns to implement fluid flow simulation with the *NVE* ensemble,

which was shown in Figure 1(c). There were three independent regions in the fluid domain: a forcing region to drive fluid flow, a temperature controlling region to control the inlet water temperature and a data collecting region to generate datasets. The fluid flow simulation was achieved by applying a constant flow-driving force F_y of 7×10^{-15} N in the y-direction to each water molecule in the forcing region (0.0 nm < y < 0.8 nm), which allowed the liquid flowed from the left boundary to the right boundary and across the periodic boundary to achieve a constant flow. In order to offset the additional energy introduced into the forcing region and ensure the energy conservation of system, the heat pump method [41–43] was introduced and the water molecules inside the temperature controlling region, ranging from 0.8 nm to 1.6 nm along the y-direction, were set at 300 K by a Langevin thermostat with a damping coefficient of 100 fs. This artificial procedure of energy addition and extraction has been reported to well match the velocity distribution of Maxwell-Boltzmann at 300 K [41]. The data collecting region was from 10 nm (y_{in}) to 30 nm (y_{out}), following the forcing region and temperature controlling region, where water molecules flowed on the graphene substrate covered by platinum particles. The time step of the simulation was set as 20 fs. Parameters such as the size of the region and the magnitude of the extra force were chosen based on parameters reported by previous work [41,44]. After the simulation system reached a steady flow state with constant centroid flow velocity, data collection was conducted during the last 200 ns. Density and velocity averaged data obtained from a 20 ns run of simulation (average data for 1×10^6 time steps) were taken as a case and 9×10^4 cases were obtained in each MD simulation.

2.3. Dataset generation and deep learning network

This section briefly introduced how datasets were generated and what was the proposal of deep learning network. More details can be consulted from the Section S1 in the Supporting Information. The present study applied deep learning on reconstructing systems of solid-liquid interface to achieve the goal that the Pt/graphene substrate structure was mapped to the water molecule transport landscape. As a result, a deep learning network was put forward, which adopted dual input and sampling channels to extract two types of point clouds and respectively represent the properties of Pt/graphene substrate and water molecules in a flexible data format (Figure 2). The related MD insufficient sampling problem for velocity field and the proposal of nanoparticle tracking optimization strategy were detailedly stated in Sections 3.2 and 3.3. We constructed four deep learning datasets (static adsorption properties of water molecule and dynamic flow properties under uniform or random distribution of Pt). The solid point cloud characterizing the Pt/graphene structure could be expressed as $\{N_1 * P_1\}$, where N_1 represented the total number of points in the solid point cloud in a sample, and P_1 represented the properties of the solid including coordinates of each point and molecular type labels. The liquid point cloud that characterized the water adsorption or water flow could be expressed as $\{N_2 * P_2\}$, where N_2 represented the total number of points in the liquid point cloud of water molecules in a sample, and P_2 represented the transportation properties of water molecules including spatial coordinates, density or velocity components in three directions of water molecules. For the four datasets, each dataset randomly produced a training set and a test set, and their ratio is 9:1 (Table 1). In order to increase the size of the

deep learning dataset, we randomly sampled a molecular dynamics simulation model with a time difference of 20 fs (one computational time step). That was, we considered Case 1 (0 ns to 20 ns) and Case 2 (20 fs to 20 ns +20 fs) as two different deep learning samples, and 9×10^4 cases were obtained in each MD model.

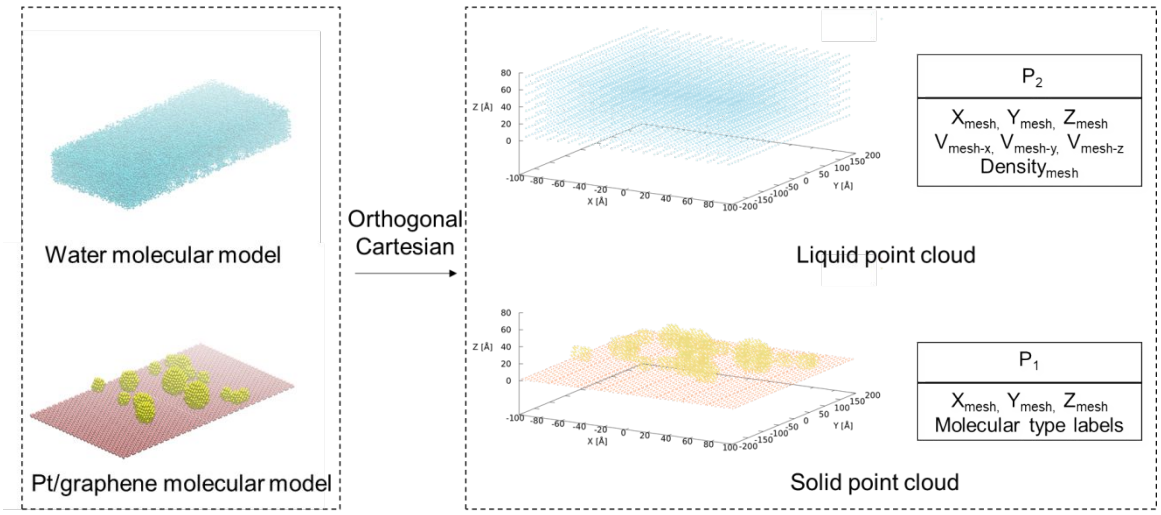

Figure 2 Generation of two types of point cloud datasets.

Our previous work has explained in detail the design, as well as advantages, of the deep learning network proposed in this work, such as the dual channel, fully connected layer shared weight, and the impact on prediction errors [45,46]. Figure 3 showed the network using two input and sampling channels to receive and process the solid and liquid point cloud, respectively. The description for the input module, sampling module, feature stitching module, and output module can be learnt from the Supporting Information in the Section S2, and the network training and testing process were stated in the Section S3 of the Supporting Information.

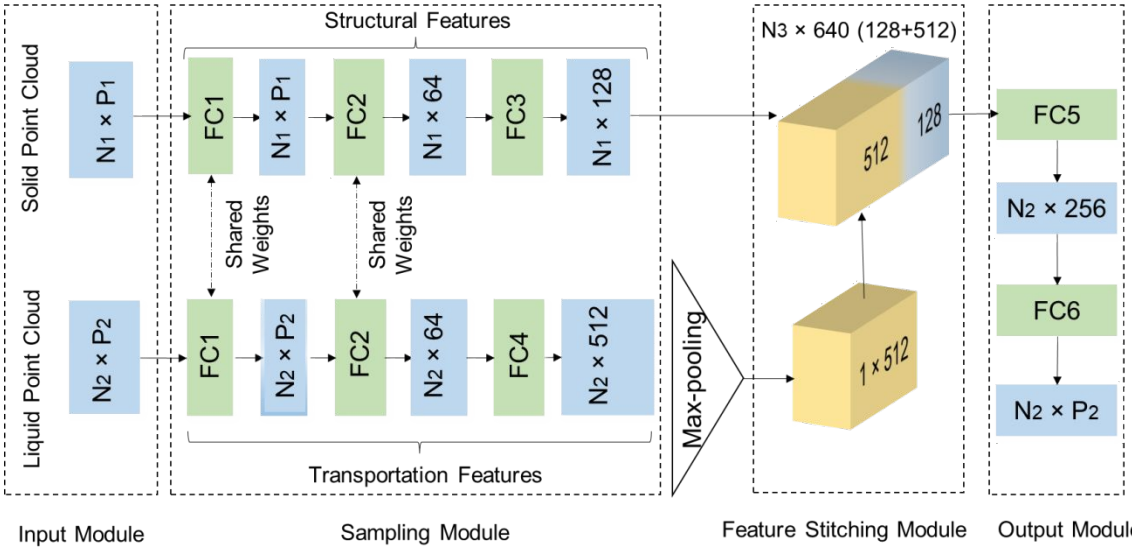

Figure 3 Construction of the deep learning network.

2.4. Evaluation of prediction performance

The error function of mean relative error (MRE) was selected to traverse the error at each mesh point, which can be used to quantitatively estimate the difference between results of MD simulation and deep learning prediction. MRE was calculated as below:

$$MRE(y,\hat{y}) = \frac{1}{N_2}\frac{\sum_{i=1}^{N}\sqrt{(y_i-\hat{y}_i)^2}}{\sqrt{y_i^2}}\times 100\% \quad (5)$$

where y was the magnitude of adsorption density or velocity on one mesh from MD simulation, $\hat{y}$ represented the corresponding predicted result of deep learning, and i represented the mesh sequence. MRE results for all samples of the test set were presented by averaging them.

For results of visualization from MD simulation and deep learning, the adsorption density and flow velocity distribution in different regions of the system were respectively displayed using 2D cross-sectional views.

To more comprehensively evaluate the prediction performance and analyze the transport mechanism, 15 cases of the test set were selected, where Pt particles uniformly distributed on the substrate. The size and number of Pt particle ranged from 2 nm to 4 nm and from 4 to 36, respectively. The overall adsorption amount and velocity of the selected models were calculated and compared to further reveal the influence of the Pt/graphene structure on the wettability and fluidity. Adsorption amount, which could quantify the Pt/graphene surface wetting state, were evaluated by estimating the total mass of water molecules within 0.66 nm of the graphene or Pt surface. The value of 0.66 nm was obtained from the first minimum of radial distribution functions of the water, $g(r)$, surrounding Pt or graphene surface as shown in Figure 4.

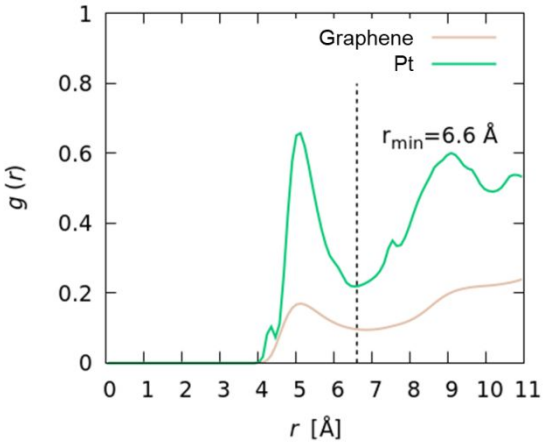

Figure 4 Radial distribution functions of the water surrounding Pt or graphene.

The average velocity components in the y-direction at denoted z coordinate positions ($v_y(z)$) were evaluated in the data collecting region from y_{in} to y_{out} by:

$$v_y(z) = \frac{\int_{y_{in}}^{y_{out}} \rho(y,z) v_y(y,z) dy}{\int_{y_{in}}^{y_{out}} \rho(y,z) dy} \quad (6)$$

where $\rho(y,z)$ and $v_y(y,z)$ were the local density and local velocity of *y*-direction components at corresponding *y* and *z* coordinates positions. Similarly, the average velocity of *x*- and *z*-direction components, marked as $v_x(z)$ and $v_z(z)$, were also calculated by Eq. (5). The overall average velocity $\overline{v}_y$ in the data collecting region were calculated by:

$$\overline{v}_y = \frac{\int_0^H v_y(z)dz}{H} \tag{7}$$

where *H* was the height of the channel in the *z*-direction.

3. Results and discussion

3.1. Prediction of the static adsorption behavior of water

Based on two physical fields (scalar field of density distribution and vector field of velocity distribution), the prediction performance of our deep learning algorithm, as well as advantages in computational cost and visual output, were discussed in the following sections by compared with previous experiments and simulations. Meanwhile, the relationship between the anisotropic wetting surface structure and the static adsorption property of liquid molecules was illustrated through prediction results of deep learning.

In Figure 5, results of MD simulation and deep learning prediction were visually compared, where the 2D density distribution of water on the *x*-*y* plane were taken from three different layers from the bottom to the top in the *z*-direction, and their quantitative analysis were conducted. The adsorption density distributions of two methods were in great agreement and the values of MRE were 8.35±3.42% and 9.56±4.97% for uniformly distributed Pt and randomly distributed Pt cases, respectively. These well consistent calculation results were analyzed to clarify the mechanism of water adsorption behavior.

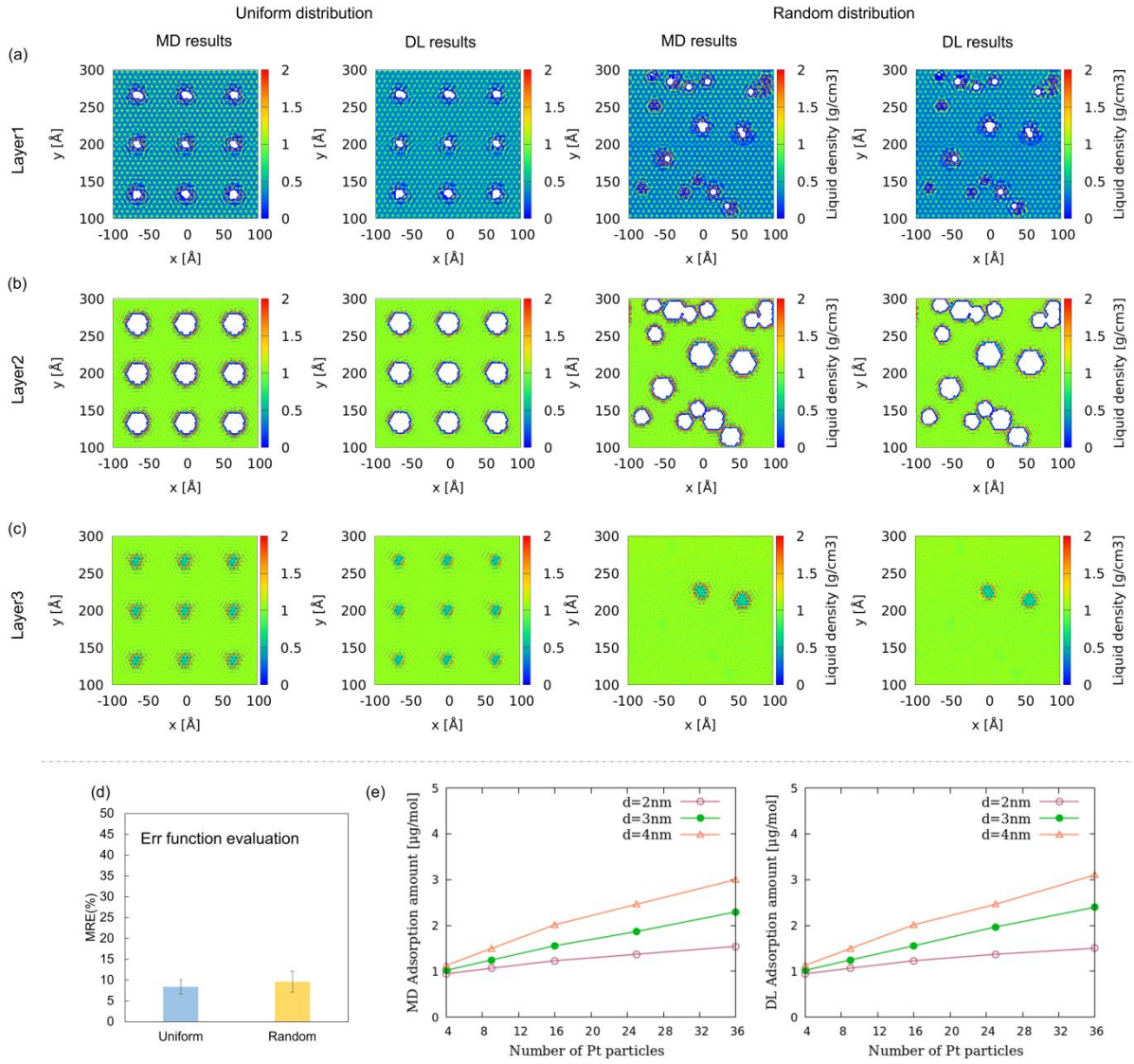

Figure 5 Results of MD simulation and deep learning (DL) prediction for visual comparison and quantitative analysis. 2D density distribution of water on the *x*-*y* plane for uniform distribution (d = 3 nm, number of Pt = 9) and random distribution of Pt at (a) layer1, (b) layer2, and (c) layer3. (d) MRE analysis. (e) The adsorption amount of water molecules on the substrate of Pt/graphene as a function of Pt number for cases with different Pt sizes.

As shown in Figure 5(a), in layer1 from the 0 (graphene surface) to 0.5 nm (*z*-direction), the density patches of liquid were concentrated on the sites of hexagon structure of graphene

surface, and therefore a regular and sparse density distribution of water molecules was observed. Higher density liquid patches appeared around the hydrophilic Pt particles than around the hydrophobic graphene surface, which indicated the packing of liquid molecules at the Pt surface. As shown in Figure 5(b), in layer2 from 1 to 1.5 nm (*z*-direction) where liquid was slightly further away from the graphene substrate, high-density patches also appeared around the Pt particles in a similar manner with the first adsorption layer. However, they were slightly lower than those in layer1 because water molecules in layer2 only adsorbed onto the Pt surface, while water molecules in layer1 were located on the junction edge between the Pt and graphene and consequently were attracted by both Pt and graphene. Moreover, a multilayer adsorption structure of liquid was generated slightly distant from Pt particles. As shown in Figure 5(c), in layer3 from the top of Pt particles to 0.5 nm above Pt particles (*z*-direction), water only gathered on the region of accessible Pt particles tips, and other regions displayed a uniform density distribution due to the disappeared interface effect of Pt. For systems with uniform distribution, water molecules were uniformly adsorbed around the Pt to form an adsorption layer structure. For systems with random distribution, when the gap between the adjacent Pt particles was too small, water molecules could not enter, and the adsorption was almost 0, which was also reproduced by our deep learning networks.

As shown in Figure 5(e), we calculated and compared the adsorption amount of water molecules on the substrate of Pt/graphene as a function of Pt number for cases with different Pt sizes, and the adsorption amounts of water calculated using two methods were also in great

agreement. With the increase of the Pt number, although the graphene surface area shrunk, the adsorption of water molecules onto the whole Pt/graphene substrate increased, which indicated the whole wettability of Pt/graphene substrate increased. Moreover, the increase of the Pt size also improved the water adsorption. The localization of water surrounding the Pt surface was since that Pt particles were hydrophilic. When the content of hydrophilic Pt particles was about 60 wt%, the adsorption amount of water molecules could reach 1.5 μg/mol at Pt particle diameter d = 2 nm (the Pt particle number was 36), while the adsorption amount of water molecules was 1.2 μg/mol at d = 4 nm (the Pt particle number was 4). Therefore, when the Pt content was the same, smaller size of Pt particles meant larger surface area of exposed Pt particles, which resulted in the larger amount of adsorbed water molecules.

3.2. Prediction of the dynamic water flow behavior

For the vector velocity field of water, the visual comparison and quantitative analysis of MRE were shown in Figure 6. MRE were 197.42±47.35% and 256.84±63.49% for uniformly distributed Pt and randomly distributed Pt cases, respectively. It is worth mentioning that using existing datasets and networks to accurately predict the velocity field of water molecules remained a challenge. We explained the reason from the data level: compared with the adsorption behavior shown in Section 3.1, the prediction error of velocity field increased significantly, which was mainly due to the difference in the source of datasets from MD simulation results of two transport behaviors. With the change of Pt/graphene structure, the water molecules in the adsorption layer showed a very regular and ordered arrangement. Therefore, the deep learning network can succeed in uncovering the relationship between the

anisotropic wetting surface structure and the adsorption behavior of water. However, the negative side of current MD simulation was its practical restriction in systems with small size (up to about 200 Å), short timescales (10^{-9} second) and drastic thermal and statistical fluctuations [47]. The discussion of the system size effect was in the Section S4 in the Support Information. As a result, the thermal fluctuations prevented us from precisely acquiring the local velocity, and the 2D velocity distribution was still noisier [38]. We tried to alter the mesh size to balance local random fluctuations of velocity according to previous multi-scale optimization strategies, which dealt with temperature distribution data [26,27]. However, since the current mesh size exceeded the maximum size value (1 Å) in previous studies, the reduction of resolution and distortion of prediction results, caused by the previous multi-scale strategy, were unacceptable and it was necessary to propose a new optimization scheme.

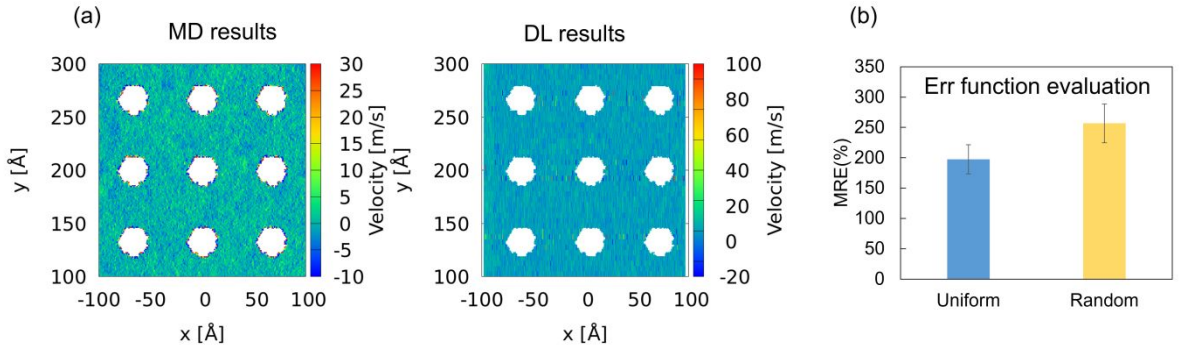

Figure 6 Visual comparison and quantitative analysis between MD simulation and DL prediction results using Cartesian grid method for the generation of datasets. (a) Visual comparison of molecular velocity distribution. (b) MRE analysis.

3.3. Nanoparticle tracking optimization strategy

The flow of water molecules exhibited the chaotic phenomenon of multi-body system, that was, local particles had random and irregular motions with uncertain and unpredictable behaviors. Researches on deep learning nowadays had achieved real-time prediction for the state evolution of large-scale spatiotemporal chaotic systems with unprecedented high-quality prediction results [48–50]. Combining these studies and the method innovation of deep learning in point cloud data processing, we proposed a nanoparticle tracking optimization strategy to improve the prediction performance of water molecular velocity field. In previous datasets, a sample was the average result of the water molecular velocity on the Cartesian grid for 20 ns (1×10^6 time steps). However, this average result did not contain the spatial coordinate information of water at each time step. The molecular interactions, as well as the molecular density characterized by molecular distribution, showed a strong correlation with the molecular velocity [51,52]. Moreover, although the molecular distribution in each time step was relatively disordered, it showed a statistically significant regularity within a longer interval. The methodology and theoretical support of nanoparticle tracking strategy was to use this real spatial distribution with statistical significance to guide the network to learn the velocity of water molecules. For the dataset, we extracted the MD simulation results of each time step from each 20 ns simulation and replaced the coordinate and velocity of each Cartesian grid in the water molecule point cloud P_2 with the real space coordinates and the corresponding velocity of each water molecule, as shown in Figure 7. Here, it should be noted that the spatial distribution of molecules could be easily obtained from the density distribution, and

the feasibility of density distribution prediction have been demonstrated in the Section 3.1. Therefore, the acquisition of molecular space coordinates would not limit the implementation of deep learning frameworks. During the training process, batch size was changed to 1024 (data of 1024 time steps was input each time) and a time window function [48,53] was added to feed the data of one batch into the network in chronological order, which prevented sample selection bias introduced by random input. Through the above operations, the spatial distribution of molecules in each time step was abstracted as a statistically significant spatial distribution within a longer interval, which could enable the guidance of the molecular spatial distribution for velocity prediction and help the network to remove the noise in the chaotic system. In addition, for a sample, compared with the original Cartesian grid method (4000000, it was equal to the total number of meshing 200×400×50) , the amount of improved point cloud data (150000, it was equal to the number of particles) was significantly reduced, which reduced the computational cost and feature extraction pressure of the network. In addition, the proposed network had good compatibility with input and output point clouds of different formats, which had also been proved in previous studies [45,54]. For testing, P_1 and the coordinates of the water molecules in P_2 at each time step within 20 ns simulation were entered, and all the output should be averaged into one prediction result.

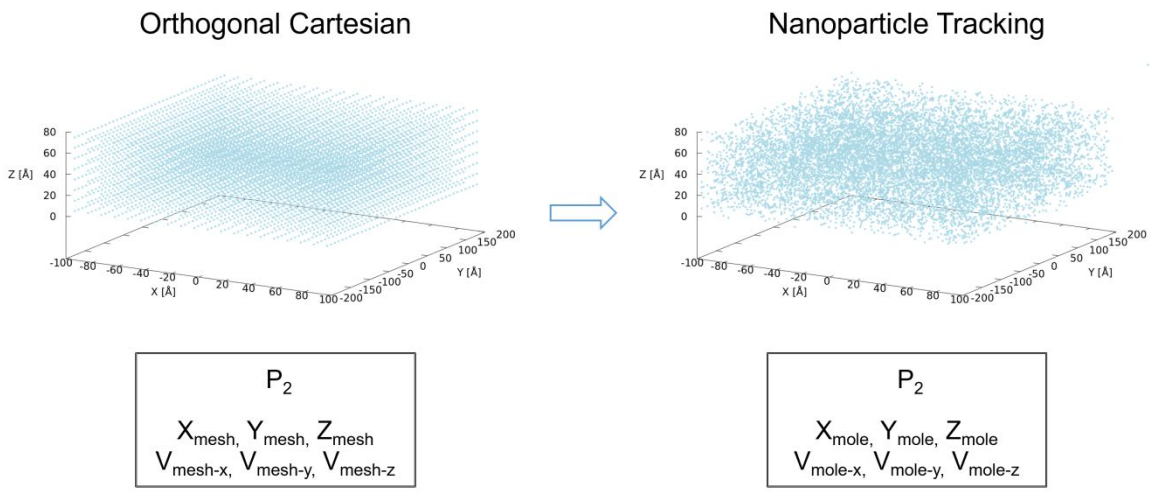

Figure 7 Nanoparticle tracking optimization strategy.

Figure 8 showed the visual comparison and quantitative analysis between the results obtained from the training and testing of nanoparticle tracking datasets, as well as the corresponding MD simulation results. MRE, as shown in Figure 8(c), decreased to 93.69± 28.42% and 117.30±33.57% for uniformly distributed Pt and randomly distributed Pt cases, respectively. Here MRE analysis using modified network was still as high as > 100%. Nevertheless, the flow of water molecules was originally the chaotic phenomenon of multi-body system, the thermal fluctuations prevented us from precisely acquiring the local velocity [52]. In addition, the numerical methods and the finite precision arithmetic of the computer also directly introduced noise into the velocity of solution, so that for practical purposes the system was irreversible although the equations of motion were reversible, and the velocity field strength must be determined by trial and error [53]. Therefore the high mean relative error of the prediction data was originated from the nosier of 2D velocity distribution obtained from the MD simulation results as indicated in the previous study. Although velocities of individual atoms were subject to error, but the previous study indicated that this did not

present a serious problems because the realistic flow patterns still emerged from the simulation [53]. It has been demonstrated that deep learning method could also reproduce some local details of MD simulation results, for example, the water flow obtained from two methods both showed a sharp change of velocity around the Pt particles, which was caused by the collision between water molecules and Pt particles. Nevertheless, only the cross-section of the first layer was shown as an example because the 2D velocity distribution on the cross-section was still noisy in MD simulations due to the thermal fluctuation and limited sampling, which was also reflected in deep learning results. For chaotic systems, we paid high attention to the overall attributes with statistical significance. Figure 8(b) displayed two-dimensional distribution (1D) velocity distribution for three velocity components in the *z*-direction and results of two methods showed great consistency. In fact, the prediction results of deep learning even showed a more stable regularity. The velocities of water flow v_y was very low near the graphene surface, and gradually increased as the water away from the graphene surface. Molecular interaction between graphene surface and water molecules was responsible for the decreased flow velocities at the surface. The water flow velocity in the region, where there were 0-3 nm Pt particles, was seemingly unstable, and the flow instabilities for water passing through a series of obstacles had also been reported in the previous study [38]. As the water flowed far away from the Pt particles, the flow velocity gradually increased and approached the classical flow behavior, because the flow was less affected by the boundary surface. Although v_x and v_z, which were not at the flow direction, were almost zero, the slight fluctuation of v_x could still be observed, associated with the

change of flow direction after the collision to obstacles.

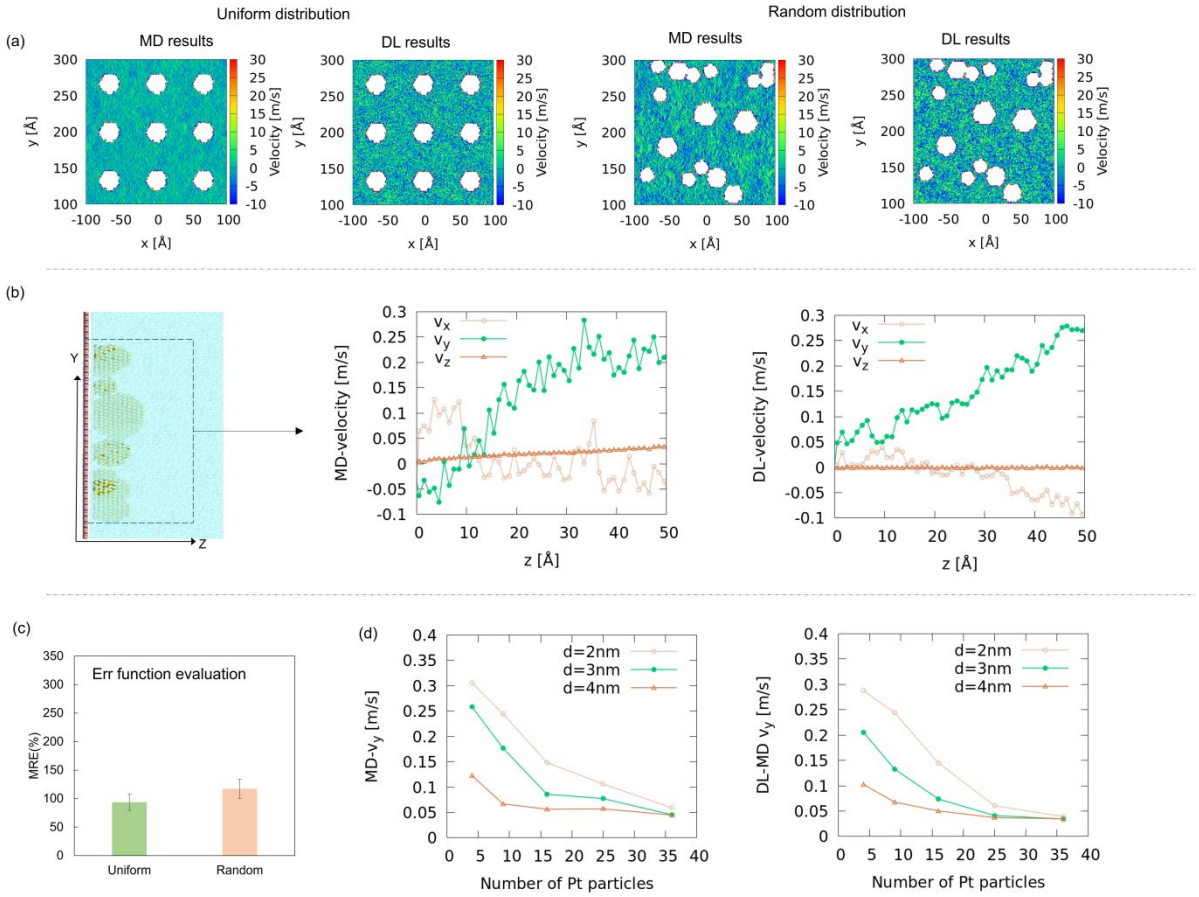

Figure 8 Visual comparison and quantitative analysis between the results obtained from the training and testing of nanoparticle tracking datasets and the corresponding MD simulation results. (a) 2D velocity distribution of water on the *x*-*y* plane for uniform distribution (d = 3 nm, number of Pt = 9) and random distribution of Pt at layer2. (b) 1D velocity distribution for three velocity components along the z direction. (c) MRE analysis. (d) The average water velocity $\overline{v}_y$ comparison in the evaluation region as a function of Pt number for cases with different Pt sizes.

Figure 8(d) showed the comparison of average water velocity $\overline{v}_y$ in the data collecting region as a function of the Pt number for cases with different Pt sizes. The average velocity of

the liquid became lower with the increase of the Pt number in the graphene substrate. Comparing among cases with different sizes of Pt particles, the increase of the Pt size resulted in that the flow velocity $\overline{v}_y$ slowed down considerably. The adverse effect of Pt particles on water flow could be divided into two aspects. Firstly, the presence of obstacles in the flow could generate eddies due to vorticity and even raise reversed flow due to that water crashed Pt blocks. Hence, with the increase of the Pt particle size and number, water flow was significantly hindered and consequently the water velocity slowed down [38]. Secondly, the strong interaction between Pt and water was beneficial for water to cling to the Pt surface. As a result, larger exposed surface area of Pt obstacles would be in favor of trapping more water molecules as surface adsorption layers, which narrowed the flow channel and reduced the velocity of water flow. When the Pt content was about 60 wt%, $\overline{v}_y$ at d = 2 nm (the Pt particle number was 36) was much lower than that at d = 4 nm (the Pt particle number was 4). We had discussed in the Section 3.1 that if the Pt content was the same, larger Pt number, but not larger Pt size, was more favorable to the increase of the exposed Pt surface area, which resulted in an increase in the overall wettability of the Pt/graphene surface, and therefore greatly blocked the water flow.

3.4. Evaluation of computing efficiency

When the training process was over, the adsorption or flow behavior of water molecules could be obtained within 1 second with the solid and liquid point clouds in the test set as input. For MD simulation, the simulation time for one model was about 5 hours with the CPU server configured as the Intel Xeon Gold 6148 2.4 Ghz × 2 CPU (320 cores). The computing

efficiency of deep learning was improved by about 18000-fold. Though it took a certain amount of time (about 60 hours) for the deep learning algorithm to train the network, only once network training needed to be conducted and so that all prediction outputs of all models in the test set can be received. Compared with the traditional experimental or simulation methods, our deep learning algorithm could visually predict the water transport landscape at the anisotropic wetting surface in real time.

3.5. Universal demonstration of proposed deep learning algorithm for nanoflow system

Deep learning algorithms based on data-driven became more and more popular in the field of engineering, physics and medicine [55–57]. In this work, deep learning was applied to model the liquid flow system on an anisotropic wetting substrate surface, to predict the water transport landscape and to reveal the flow mechanism at the nanoscale under the molecular interaction between water and Pt/graphene surface. The feature point of the collaboration research of MD simulation and deep learning is to effectively extract a large number of micro-features of liquid and anisotropic wetting surface of solid. In the present study, the point feature of water molecules and Pt/graphene substrate with micro geometry was extracted as input, and the static and dynamic properties of water molecules at the nanoscale as output. Our proposed deep learning algorithm had strong universality and succeeded in the application of predicting water static and dynamic properties for systems with different input of control variables. The atomic species and 3D spatial coordinates in the solid cloud P_1 acted the role of fixed inputs. For the regularly distributed scalar density field of water adsorption, the Cartesian meshing result and the corresponding density in the liquid point cloud P_2 were

used as the input. For the locally disordered vector velocity field, the real spatial coordinates of water molecules in P_2 in the nanoparticle tracking datasets and the corresponding 3D velocity components were used as inputs. In this work, input control variables of the network, that was the attributes of point cloud, were up to but not limited to 11, including Pt and graphene types and 3D coordinates, 3D coordinates and 3D velocity components of water molecules, and output results of prediction were chosen as scalar or 3D vector as needed. Looking ahead to the future work, we could apply our algorithm on the prediction of micro-scale transport of other molecules, such as polymer acting as the liquid point cloud P_1. In such case, molecular type labels (0, 1 and 2) could be used to represent Pt, graphene and polymer. In addition, some real properties of polymer molecules, such as the steric configuration, the bond angle, the bond energy and the charged properties of atoms/molecules, could play the role of the input to build a more real deep learning dataset. For example, when considering the charge properties of atoms/molecules, we could add a dimension to P_1 which was the amount of charge carried by each atom on the substrate. Alternatively, we could populate this dimension with the external electric field values (of the same value) of the system as a whole. Exactly which option could lead to better predictive performance was subject to experimental verification but was methodologically feasible and easy to implement. The Cartesian meshing results and corresponding polymer concentrations in P_2 were also used as inputs. All in all, to improve the performance of our current micro/nanofluidic predictions and predict flow behaviors of macromolecules, more technical details need further exploration.

4. Conclusion

In this work, a customized framework of deep learning was proposed to uncover the flow and adsorption mechanism of water at anisotropic wetting surface. Taking different input parameters into account, our framework of deep learning can efficiently distinguish the local wettability according to the surface pattern of Pt/graphene substrate with a high level of precision and visually display the distribution of scalar adsorption density, as well as the vector velocity field of fluid flow, which can efficiently promote the development of current experiments and simulations. Furthermore, we demonstrated the extension potential of the proposed framework of deep learning in studying the micro flow phenomena of complicated molecules. We expected that deep learning method can be beneficial for the fabrication and development of nanofluidic devices.

Acknowledgements

This work was supported by JST CREST Grant Number JPMJCR17I2, Japan. It was performed on the Supercomputer system “AFI-NITY” at the Advanced Fluid Information Research Center, Institute of Fluid Science, Tohoku University.

Reference

1 W. Sparreboom, A. van den Berg and J. C. T. Eijkel, *Nature nanotechnology*, 2009, **4**, 713–720.

2 S. Kumar Kannam, B. D. Todd, J. S. Hansen and P. J. Daivis, *The Journal of chemical physics*, 2012, **136**, 24705.

3 M. Majumder, N. Chopra, R. Andrews and B. Hinds, *Nature*, 2005, **438**, 930.

4 J. K. Holt, H. G. Park, Y. Wang, M. Stadermann, A. B. Artyukhin, C. P. Grigoropoulos, A. Noy and O. Bakajin, *Science*, 2006, **312**, 1034–1037.

5 M. H. Köhler, J. R. Bordin, C. F. de Matos and M. C. Barbosa, *Chemical Engineering Science*, 2019, **203**, 54–67.

6 M. Whitby, L. Cagnon, M. Thanou and N. Quirke, *Nano letters*, 2008, **8**, 2632–2637.

7 Z. Y. Liu, L. Chen and H. Chen, *Heat Transfer Engineering*, 2022, 1–10.

8 M. An, H. Wang, Y. Yuan, D. Chen, W. Ma, S. W. Sharshir, Z. Zheng, Y. Zhao and X. Zhang, *Surfaces and Interfaces*, 2022, **28**, 101690.

9 G. Hummer, J. C. Rasaiah and J. P. Noworyta, *nature*, 2001, **414**, 188–190.

10 S. Joseph and N. R. Aluru, *Nano letters*, 2008, **8**, 452–458.

11 J. A. Thomas and A. J. H. McGaughey, *Physical review letters*, 2009, **102**, 184502.

12 A. Kalra, S. Garde and G. Hummer, *Proceedings of the National Academy of Sciences*, 2003, **100**, 10175–10180.

13 G. Zhao, X. Li, M. Huang, Z. Zhen, Y. Zhong, Q. Chen, X. Zhao, Y. He, R. Hu, T. Yang

and others, *Chemical Society Reviews*, 2017, **46**, 4417–4449.

14 L. Yao, Z. Ou, B. Luo, C. Xu and Q. Chen, *ACS central science*, 2020, **6**, 1421–1430.

15 S. Zhao, Y. Yang and Z. Tang, *Angewandte Chemie*, 2022, **134**, e202110186.

16 Y. Guo, H. Sun, X. Zhang, S. Wang and G. Li, in *Reference Module in Chemistry, Molecular Sciences and Chemical Engineering*, Elsevier, 2023.

17 G. Li, J. Ji, J. Ni, S. Wang, Y. Guo, Y. Hu, S. Liu, S. F. Huang and Y. Y. Li, *Science of The Total Environment*, 2022, **813**, 151920.

18 K. B. Newhart, R. W. Holloway, A. S. Hering and T. Y. Cath, *Water Research*, 2019, **157**, 498–513.

19 J. Zhuang, J. Sun and G. Yuan, *Neural Computing and Applications*, 2021, 1–12.

20 G. Li, K. Watanabe, H. Anzai, X. Song, A. Qiao and M. Ohta, *Scientific reports*, 2019, **9**, 1–11.

21 G. Li, X. Song, A. Qiao and M. Ohta, *Computer Modeling in Engineering \& Sciences*, 2018, **117**, 143–155.

22 S. Wang, D. Wu, G. Li, X. Song, A. Qiao, R. Li, Y. Liu, H. Anzai and H. Liu, *Computer Methods and Programs in Biomedicine*, 2022, **216**, 106664.

23 G. Li, Y. Zhu, Y. Guo, T. Mabuchi, D. Li, S. Huang, S. Wang, H. Sun and T. Tokumasu, *ACS Applied Materials & Interfaces*, 2023, **15**,5099–5108.

24 X. Ding, Y. Zhang, J. Li, B. Mao, Y. Guo and G. Li, *Internet of Things*, 2023, **21**, 100689.

25 X. Qian and R. Yang, *Materials Science and Engineering: R: Reports*, 2021, **146**, 100642.

26 G. Li, Y. Guo, T. Mabuchi, D. Surblys, T. Ohara and T. Tokumasu, *Journal of Molecular*

Liquids, 2022, **349**, 118489.

27 Y. Guo, G. Li, T. Mabuchi, D. Surblys, T. Ohara and T. Tokumasu, *Journal of Colloid and Interface Science*, 2022, **613**, 587–596.

28 Y. Guo, D. Surblys, Y. Kawagoe, H. Matsubara, X. Liu and T. Ohara, *International Journal of Heat and Mass Transfer*, 2019, **135**, 115–123.

29 Y. Guo, D. Surblys, Y. Kawagoe, H. Matsubara and T. Ohara, *Journal of Applied Physics*, 2019, **126**, 185302.

30 Y. Guo, D. Surblys, H. Matsubara, Y. Kawagoe and T. Ohara, *The Journal of Physical Chemistry C*, 2020, **124**, 27558–27570.

31 Y. Guo, D. Surblys, H. Matsubara and T. Ohara, *Journal of Molecular Liquids*, 2021, **335**, 116243.

32 L. Qiu, F. Li, N. Zhu, Y. Feng, X. Zhang and X. Zhang, *International Journal of Heat and Mass Transfer*, 2022, **184**, 122280.

33 Y. Guo, T. Mabuchi, G. Li and T. Tokumasu, *Macromolecules*, 2022, **55**, 4245–4255.

34 T. Mabuchi, S. F. Huang and T. Tokumasu, *Macromolecules*, 2020, **54**, 115–125.

35 T. Mabuchi, S. F. Huang and T. Tokumasu, *Macromolecules*, 2020, **53**, 3273–3283.

36 T. Mabuchi, S. F. Huang and T. Tokumasu, *Journal of Polymer Science*, 2020, **58**, 487–499.

37 W. Gonçalves, T. Mabuchi and T. Tokumasu, *The Journal of Physical Chemistry C*, 2019, **123**, 28958–28968.

38 D. C. Rapaport, *Physical Review A*, 1987, **36**, 3288–3299.

39 J. Michalowsky, L. V Schäfer, C. Holm and J. Smiatek, *The Journal of Chemical Physics*, 2017, **146**, 54501.

40 B. Shi and V. K. Dhir, *The Journal of chemical physics*, 2009, **130**, 34705.

41 D. C. Marable, S. Shin and A. Yousefzadi Nobakht, *International Journal of Heat and Mass Transfer*, 2017, **109**, 28–39.

42 Q. Weilin, Gh. Mohiuddin Mala and L. Dongqing, *International Journal of Heat and Mass Transfer*, 2000, **43**, 353–364.

43 A. J. Markvoort, P. A. J. Hilbers and S. V Nedea, *Physical review E*, 2005, **71**, 66702.

44 P. Chakraborty, T. Ma, L. Cao and Y. Wang, *International Journal of Heat and Mass Transfer*, 2019, **136**, 702–708.

45 G. Li, H. Wang, M. Zhang, S. Tupin, A. Qiao, Y. Liu, M. Ohta and H. Anzai, *Communications biology*, 2021, **4**, 1–12.

46 C. R. Qi, H. Su, K. Mo and L. J. Guibas, in *Proceedings of the IEEE conference on computer vision and pattern recognition*, 2017, 652–660.

47 J. Koplik, J. R. Banavar and J. F. Willemsen, *Physics of Fluids A: Fluid Dynamics*, 1989, **1**, 781–794.

48 J. Pathak, B. Hunt, M. Girvan, Z. Lu and E. Ott, *Physical review letters*, 2018, **120**, 24102.

49 J. Pathak, A. Wikner, R. Fussell, S. Chandra, B. R. Hunt, M. Girvan and E. Ott, *Chaos: An Interdisciplinary Journal of Nonlinear Science*, 2018, **28**, 41101.

50 F. Cichos, K. Gustavsson, B. Mehlig and G. Volpe, *Nature Machine Intelligence*, 2020, **2**, 94–103.

51 H. Sun, Z. Liu, G. Xin, Q. Xin, J. Zhang, B.-Y. Cao and X. Wang, *Numerical Heat Transfer, Part A: Applications*, 2020, **78**, 231–251.

52 H. Sun and M. Wang, *Journal of Molecular Liquids*, 2022, **345**, 117872.

53 W. S. Lee and S. Flach, *Machine Learning: Science and Technology*, 2020, **1**, 45019.

54 G. Li, X. Song, H. Wang, S. Liu, J. Ji, Y. Guo, A. Qiao, Y. Liu and X. Wang, *Frontiers in Physiology*, 2021, **12**, 733444.

55 S.-C. Wang, Y. T. Tsai and Y.-S. Ciou, *Journal of Industrial Information Integration*, 2020, **20**, 100177.

56 A. Abdollahzadeh, I. Belevich, E. Jokitalo, A. Sierra and J. Tohka, *Communications biology*, 2021, **4**, 1–14.

57 M. Javaid, A. Haleem, R. P. Singh and R. Suman, *Journal of Industrial Integration and Management*, 2021, **06**, 429–447.